Ligand Protonation at Carbon, not Nitrogen, During H_2 Production with Amine-Rich Iron Electrocatalysts

Práxedes Sánchez,[†§] Bhumika Goel,[†§] Hagen Neugebauer,[‡§] Roger A. Lalancette,[†] Stefan Grimme,[‡] Andreas Hansen,[‡*] and Demyan E. Prokopchuk[†*]

[†] Department of Chemistry, Rutgers University-Newark, 73 Warren Street, Newark, NJ 07102, United States

[‡]Mulliken Center for Theoretical Chemistry, Institut für Physikalische und Theoretische Chemie, Rheinische Friedrich-Wilhelms Universität Bonn, Beringstraße 4, 53115 Bonn, Germany

KEYWORDS : electrocatalysis, hydrogen, iron, ligand design, quantum chemistry

ABSTRACT: We present monometallic H_2 production electrocatalysts containing electron rich triamine-cyclopentadienyl (Cp) ligands coordinated to iron. After selective CO extrusion from the iron tricarbonyl precursors, electrocatalysis is observed via cyclic voltammetry in the presence of exogenous acid. Contrary to the fact that amines in the secondary coordination sphere are often protonated during electrocatalysis, comprehensive quantum chemical calculations indicate that the amines likely do not function as proton relays; instead, *endo*-Cp ring protonation is most favorable after $1e^-$ reduction. This unusual mechanistic pathway emphasizes the need to consider a broad domain of H^+/e^- addition products by synergistically combining experimental and theoretical resources.

INTRODUCTION

Earth-abundant metals (EAMs) are essential to life, catalyzing complex redox reactions involving multiple protons and electrons. In Nature, [Fe-Fe] and [Ni-Fe] hydrogenases use azadithiolate and arginine moieties, respectively, to shuttle protons between the metal's primary coordination sphere and these nitrogen bases.[1] Consequently, this behavior has inspired the development of synthetically tractable electrocatalyst biomimics containing amine moieties capable of facilitating proton movement for H_2 production and/or oxidation using EAMs.[2] As ligand designs for fuel-forming electrocatalysis are refined to incorporate secondary coordination sphere interactions,[3] mechanistic scenarios become increasingly complicated due to multiple donor/acceptor moieties mediating the movement of protons and electrons. Thus, synergistic cooperation between experimentalists and theoreticians is essential to identify plausible mechanistic pathways and avoid energy pitfalls that could stifle catalytic activity.[2c,4]

While η^5-C_5H_5 (Cp) and electron-rich η^5-C_5Me_5 (Cp*) often function as ancillary ligands, they can also participate in C-H bond activation reactions.[5] Mechanistic studies have proposed the existence of η^4-CpH or η^4-Cp*H intermediates using Co,[6] Rh,[7], Re[8], and *f*-block[9] complexes, and there is synthetic precedent for η^4-Cp ligation at Fe,[10] Co,[11] and Rh.[11a,12] Experimental and computational analyses have demonstrated that active participation of the Cp/Cp* ligand can be essential in the context of proton-coupled electron transfer (PCET),[6,13] driving the need to evaluate new Cp derivatives for small molecule activation and catalysis.

In contrast, amine-functionalized Cp ligands remain underexplored for applications in catalysis.[14] Notably, the electron rich triamine-cyclopentadienylium ligand $^{en}Cp^{NHiPr+}$ (**1**, Scheme 1; en = *N,N'*-dimethylethylenediamine) was used to synthesize a piano-stool iron carbonyl complex which catalyzes the reductive amination of secondary amines.[14c] Computational studies suggested that a pendant amine on ligand **1** facilitates proton transfer during substrate reduction, inspiring us to synthesize a library of $^{en}Cp^{R+}$ ligands for applications in H_2 production electrocatalysis (Scheme 1). Due to the multitude of potential protonation sites, we rationalized that comprehensive multi-level modeling methods[15] considering conformational flexibility, tautomers, and solvent/solute interactions should be utilized to understand the experimental results.

We describe the synthesis, electrochemistry, H_2 production electrocatalysis, and quantum chemical modeling of Fe complexes with the electron rich triamine-cyclopentadienyl ligand $^{en}Cp^{R}$ (R = NH^iPr, pyrrlolidinyl , NHBn). Surprisingly, thermochemical landscape analysis reveals that direct protonation of the Cp ring is most favorable, generating a key *endo*-Fe(η^4-CpH) intermediate. Therefore, the experimental

Scheme 1. Synthesis of Fe complexes.

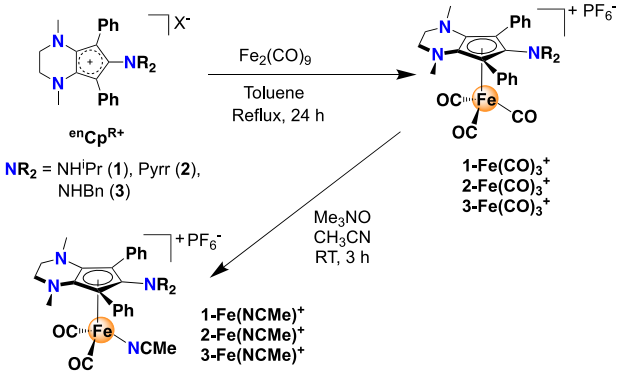

and computational data collectively suggest that the pendant amines behave as *ancillary* electron-rich functional groups, providing evidence that amines may not always function as proton relays due to pK_a mismatches between the exogenous proton source and amine functionalities.

RESULTS AND DISCUSSION

The amine-functionalized cyclopentadienylium salts **1** and **2** (**^{en}Cp^{R+}**; R = NH^{i}Pr, Pyr) were prepared as previously reported[16] while ligand **3** (R = NHBn) was prepared using a similar protocol (Scheme 1). Reaction of these salts in refluxing toluene with $Fe_2(CO)_9$ yields air stable Fe(II) tricarbonyl complexes **1-Fe(CO)$_3^+$**,[14c] **2-Fe(CO)$_3^+$**, and **3-Fe(CO)$_3^+$** which were isolated as PF_6^- salts after workup. X-ray crystallography reveals isostructural motifs for all three complexes, with nearly equidistant C-C bond lengths connecting the carbon atoms within the Cp ring (Fig S11). When compared to the CO stretching frequencies of Cp*Fe(CO)$_3^+$ (ν_{CO} = 2130, 2078 cm^{-1}; Nujol),[17] solid-state IR data for **1-Fe(CO)$_3^+$** exemplifies the potent electron donor ability of these **^{en}Cp^R** ligands (ν_{CO} = 2048, 1969 cm^{-1}; KBr).

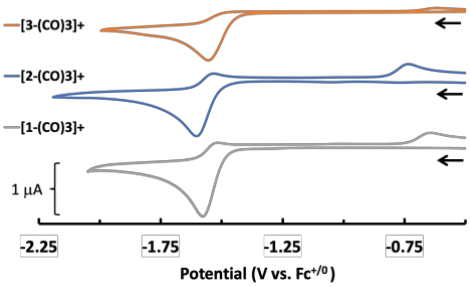

Fig 1. CVs of 1-Fe(CO)$_3^+$, 2-Fe(CO)$_3^+$, and 3-Fe(CO)$_3^+$. Conditions: CH_3CN, 0.1 M [Bu$_4$N][PF_6], 1.0 mM analyte, 100 mV/s.

Cyclic voltammograms (CVs) for complexes **1-Fe(CO)$_3^+$**, **2-Fe(CO)$_3^+$**, and **3-Fe(CO)$_3^+$** are shown in Fig 1 and data are summarized in Table 1. All three complexes exhibit partially reversible or irreversible redox features, whose currents and potentials remain constant with repeated linear potential sweeps. Although the pendant amines vary with respect to sterics and electronics, there is a reduction peak around E_{pc} = -1.6 V in all three cases, attributed to a diffusion-controlled 1e$^-$ reduction event which becomes more reversible with faster scan

Table 1. Electrochemical Data for Fe(CO)$_3^+$ complexes.

Complex	$E_{1/2}$ (V)[a]	E_{pa} (V)[a]	k_{CO} (s^{-1})
1-Fe(CO)$_3^+$	-1.59 (-1.25)	-0.62 (-0.61)	2.0 ± 1.1
2-Fe(CO)$_3^+$	-1.57 (-1.22)	-0.72 (-0.59)	6.0 ± 1.4
3-Fe(CO)$_3^+$	-1.55 (-1.23)	-0.60 (-0.60)	11.9 ± 3.6

[a]DFT-calculated redox potentials ($E_{1/2}$) in parentheses.

rates (Fig S16). In all three cases, this behavior is generally described by an EC reaction mechanism where the rapid, reversible reduction of **[Fe](CO)$_3^+$** is followed by irreversible CO loss to generate the neutral Fe dicarbonyl intermediate **[Fe](CO)$_2$** (Scheme 2, top). The rate of CO dissociation (k_{CO}) was calculated by plotting the change in cathodic peak potential (E_{pc}) versus the natural logarithm of inverse scan rate (ln(1/v)), (Eqn S1).[18] Complexes **1-Fe(CO)$_3^+$** and **2-Fe(CO)$_3^+$** have similar CO dissociation rate constants (k_{CO} = 2.0 ± 1.1 and 6.0 ± 1.4 s^{-1} respectively) while **3-Fe(CO)$_3^+$** is significantly faster (k_{CO} = 11.9 ± 3.6 s^{-1}). Since the redox potentials for all three complexes are extremely similar, the bulkier benzyl group on **3-Fe(CO)$_3^+$** suggests that ligand sterics may enhance the rate of CO dissociation. These k_{CO} values are all much lower than observed for the rate of CO loss from tricarbonyl complex $CpFe(CO)_3$ ($k_{CO} \geqq 10^3$ s^{-1}), which undergoes a strictly dissociative mechanism upon reduction (i.e., no $\eta^5 \rightarrow \eta^3$ ring slippage).[19] For these new Fe complexes, computational data suggest that a formally 19e$^-$ intermediate is avoided by a ring slip (haptotropic shift) upon reduction, generating an unusual Fe(η^2-**^{en}Cp^R**) intermediate (Scheme 2, right and Fig S24). However, the DFT-calculated potentials for 1e$^-$ reduction of **1-Fe(CO)$_3^+$, 2-Fe(CO)$_3^+$**, and **3-Fe(CO)$_3^+$** are anodically shifted by ca. +0.3 V compared to experiment. If rapid ring slippage were to occur upon 1e$^-$ reduction, the decrease in coordination number would anodically shift the observed redox potential as predicted by the DFT calculations (see SI for discussion). Therefore, the experimental data suggests that electron transfer is rapid and subsequent ring slippage is slow, leading to more negative observed redox potentials and retention of the η^5-**^{en}Cp^R** coordination mode on the electrochemical timescale.[20] Finally, an irreversible oxidation observed at E_{pa} = -0.6 to -0.7 V is postulated to be re-oxidation of the neutral Fe^I dicarbonyl intermediate **[Fe](CO)$_2$** followed by irreversible coordination of MeCN, which is in excellent agreement with experiment (Table 1).

Scheme 2. Elementary steps showing irreversible CO loss by an EC mechanism followed by solvent uptake after re-oxidation (left) with computed η^2-(**^{en}Cp^R**) intermediate 1-Fe(CO)$_3$ (right) [a]

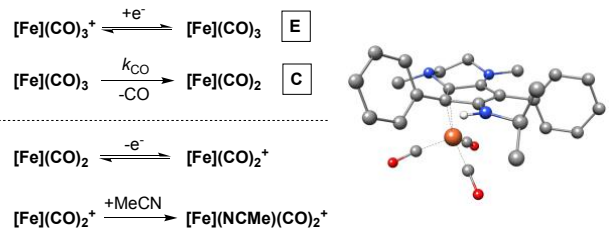

[a][Fe] = Fe(^{en}**Cp^R) where R = NH^{i}Pr, Pyr, Bn.**

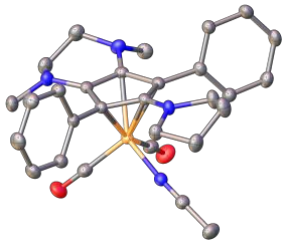

Fig 2. X-ray crystallographic structure of **2-Fe(NCMe)$^+$** with 50% probability ellipsoids. Hydrogen atoms and PF_6^- are omitted for clarity.

Based on previous electrochemical studies using $[CpFeL(CO)_2]^+$ and $CpFeX(CO)_2$ complexes,[21] loss of L or X from these coordinatively saturated piano stool complexes is a prerequisite for H_2 production. Thus, a CO ligand is extruded by treatment with 1 equiv Me_3NO to generate the 18e$^-$ adducts **1-Fe(NCMe)$^+$**, **2-Fe(NCMe)$^+$**, and **3-Fe(NCMe)$^+$** (Scheme 1). The structural assignment of **2-Fe(NCMe)$^+$** was confirmed by

single crystal X-ray diffraction (Fig 2). CVs of these three complexes in acetonitrile show broadened and partially reversible redox waves, attribute to an EC mechanism with reversible solvent binding at iron (Fig S18 (black trace)).[18b] This behavior has been studied in depth using [CpCo(diphosphine)(NCMe)]$^+$ salts, where the NCMe dissociation rate constant is on the order of 10^4-10^7 s^{-1} in non-coordinating solvents.[6,18a] CVs of **1-Fe(NCMe)$^+$**, **2-Fe(NCMe)$^+$**, and **3-Fe(NCMe)$^+$** in fluorobenzene at 100 mV/s reveal loss of the anodic feature, qualitatively indicating that solvent loss is facile upon electrochemical reduction (Fig S22). In addition, the observed redox potentials in acetonitrile are in good agreement with theory (Table 2).

Next, these dicarbonyl solvento adducts were tested for H_2 production electrocatalysis with the exogenous acid 4-methyl-*N*-tosylbenzenesulfonamide (Tos_2NH, pK_a^{MeCN} = 11.97).[22] Initial screening with 20 mM acid reveals an S-shaped current response at cathodic potentials, whose plateau current (i_{cat})

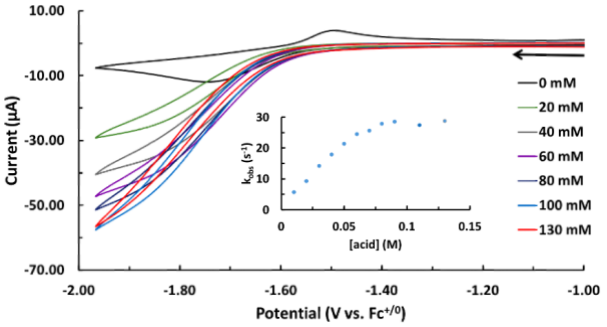

Fig 3. CVs of **1-Fe(NCMe)$^+$** with increasing concentrations of Tos_2NH. Conditions: CH_3CN, 0.1 M [Bu_4N][PF_6], 1.0 mM analyte, 800 mV/s. Inset: dependence of k_{obs} on acid concentration.

becomes independent of scan rate at ≧ 800 mV/s (Fig S17).[18b] The relatively shallow slopes may be due to slow electron transfer from the electrode to the metal complex (Fig S18).[23] For **1-Fe(NCMe)$^+$**, successive additions of acid trigger the appearance of increased peak currents, attributed to H_2 production at a half-wave catalytic potential ($E_{cat/2}$) of –1.72 V (Fig 3). When Tos_2NH < 70 mM, there is a linear dependence between k_{obs} and [acid], indicating a first-order dependence on [acid]. When [Tos_2NH] > 70 mM, the observed rate constant k_{obs} becomes independent of [acid], with the maximum observed turnover frequency for H_2 production calculated to be 29 s^{-1}.

The reaction is first order in catalyst, displaying a linear dependence on [Fe] with constant [acid] (Fig S19). Importantly, CV control experiments comparing 20 mM Tos_2NH solutions in the absence and presence of **1-Fe(NCMe)$^+$** clearly indicate that the Fe catalyst is responsible for the observed current enhancement (Fig S20). Using a weaker acid such as $HNEt_3^+$ (pK_a^{MeCN} = 18.82)[26] results in no current enhancement in CV traces, indicating that stronger acids are essential for H_2 production to occur in the applied potential window (Fig S21).

Table 2. Electrocatalysis Data for Fe(NCMe)$^+$ complexes.

Complex	$E_{1/2}$ (V)[a]	$E_{cat/2}$ (V)	k_{cat} (s^{-1})	η (V)	FE (%)
1-Fe(NCMe)$^+$	-1.61 (-1.76)	-1.72	29	0.98	65 ± 3
2-Fe(NCMe)$^+$	-1.61 (-1.67)	-1.76	35	1.02	65 ± 3
3-Fe(NCMe)$^+$	-1.58 (-1.74)	-1.72	45	0.98	64 ± 1

[a]Calculated redox potentials ($E_{1/2}$) in parentheses (vide infra).

Table 2 summarizes the electrocatalysis data. Similar turnover frequencies, modest Faradaic efficiencies,[24] and similar overpotentials (η)[25] are found for this triad, suggesting that the amine variation has a minimal effect on catalytic activity. "Rinse test" electrolysis following a typical controlled potential electrolysis trial indicates that the Fe complexes are mainly responsible for H_2 production (Fig S24 and Table S2).[24]

For the DFT calculations a multi-level protocol was employed, where different levels of theory were used at different steps to obtain reliable free energy estimates with best efficiency (Fig 4). Structure ensembles were generated by CREST[27] with the semi empirical quantum mechanical (SQM) GFN2-xTB[28] method. The low computational costs of GFN2-xTB allow extensive exploration of the chemical space on a quantum mechanical level. The structures lowest in energy were picked and optimized with the efficient composite r^{2}SCAN-3c[29] DFT method in combination with the implicit solvation model DCOSMO-RS[30] to account for solvation effects in the geometry. Employing these optimized structures, higher level single point energy calculations were performed with r^{2}SCAN-D4[31] and the extensive def2-QZVPP[32] basis set. Secondly, the recently developed single-point Hessian approach[33] was applied in combination with GFN2-xTB to calculate vibrational frequencies and obtain modified rigid-rotor-harmonic-oscillator (mRRHO) thermostatistical contributions at an accurate and cost-efficient level. Adding the

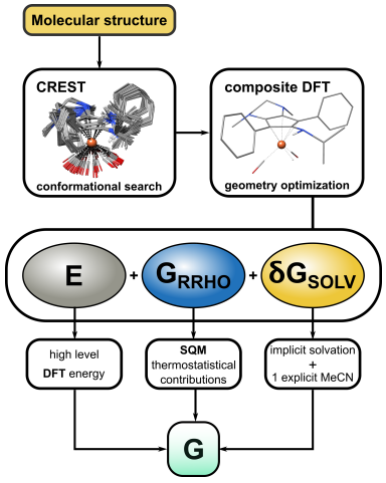

Fig 4. Computational multi-level protocol employed to generate accurate free energies.

solvation contribution calculated with the implicit COSMO-RS[34] solvation model results in the total free energy calculated with excellent efficiency[35] (see SI for details).

To assess the range of possible reaction pathways, a ground-state free energy landscape was surveyed. Complex **1-Fe(NCMe)$^+$** is used as a test case to rationalize the observed electrocatalytic behavior under the assumption that the thermochemically preferred protonation sites are also kinetically facile (Fig 5, top).[4] The 3D graphical representation of the ground state thermochemical data plots the overall

charge, number of hydrogen atoms, and ground state free energies for selected H^+/e^- addition products, with a total of 44 possible intermediates considered in this study. The SI contains a more detailed 3D graph along with free energy data for all intermediates (Fig S28-S31).[25] Inspecting structures with a +2 charge (yellow bars) indicates that protonation prior to reduction is unfavorable (+20.2 to +64.9 kcal/mol), with the first step instead being $1e^-$ reduction to generate the solvento adduct **1-Fe(NCMe)** (+23.7 kcal/mol) as denoted by a red arrow. By interrogating the lowest energy pathway for addition of H^+/e^- prior to releasing H_2, the catalyst likely operates by an ECEC mechanism (E = electrochemical step, C = chemical (H^+ addition) step) and is distilled into a 2D energy profile at the bottom of Fig 5. After initial reduction, solvent loss to produce **1-Fe** is exergonic (+15.4 kcal/mol; ΔG = -8.3 kcal/mol), consistent with the irreversible dissociation of acetonitrile from **1-Fe(NCMe)** when non-coordinating solvents are used (vide infra).

A structural summary of the proposed ECEC mechanism is shown in Scheme 3, where redox potentials and pK_a values are calculated from the computed free energies (Fig S28-S30). Reduction of **1-Fe(NCMe)**$^+$ generates a mixture of **1-Fe** and **1-Fe(NCMe)**, the former of which is thermodynamically favorable; however both are considered plausible intermediates since these thermochemical landscape analyses do not consider reaction kinetics.[36] Next, direct protonation of the metal center is disfavored because it is endergonic by +3.3 kcal/mol in the presence of Tos_2NH (pK_a = 9.6; Fig S28). Instead, *endo*-CH protonation of the Cp carbon atoms containing the phenyl moieties is exergonic by 5.1 kcal/mol, generating **1-Fe(NCMe)(endo-CpH)**$^+$ (pK_a = 15.7), which is significantly more favorable than protonation at any of the amines or protonation at any other Cp ring position (Fig S29). Next, reduction and ligand-to-metal tautomerization is exergonic by 9.5 kcal/mol, generating the neutral hydride complex **1-FeH** (pK_a = 33.4) with subsequent loss of acetonitrile (Scheme 3, bottom). This computed acidity is significantly lower than the experimentally derived acidity of $FeHCp^*(CO)_3$ (pK_a^{MeCN} = 25.7), reflecting the markedly stronger donor character of $^{en}Cp^{NHiPr}$ vs. the Cp* ligand. Importantly, protonation of the metal center to generate an Fe^{IV} dihydride intermediate can also be excluded based on its high acidity (pK_a = -0.8). Direct protonation of the hydride produces **1-Fe(H$_2$)**$^+$ (pK_a = 9.6), more favorable than protonation of the amine to yield **1-FeH(NH)**$^+$ by three orders of magnitude (pK_a = 6.3). Consequently, this disfavors a classic bifunctional/heterolytic H_2 evolution pathway[37] on thermochemical grounds due to a pK_a mismatch between the proton source and pendant amine. Replacing H_2 for NCMe is exergonic by 4.0 kcal/mol, regenerating **1-Fe(NCMe)**$^+$ (Fig 5).

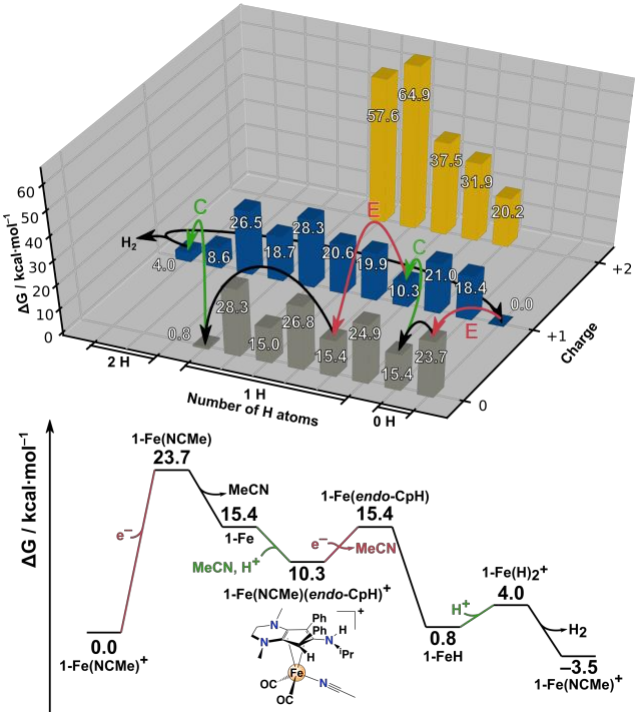

Fig 5. Top: Partial ground state 3D free energy landscape (kcal mol^{-1}) for electrocatalytic H_2 production with arrows representing most favorable reduction and protonation steps. Free energies are all referenced to complex **1-Fe(NCMe)**$^+$ (0.0 kcal/mol), where the acid source is incorporated by adding the electrochemical free energy term $\Delta G = -nFE$ where n = number of electrons, F = Faraday constant, and E is the standard state thermodynamic potential in acetonitrile for the reaction $2Tos_2NH + 2e^- \rightleftharpoons H_2 + 2Tos_2N^-$ ($E°_{H+/H2}$ = -0.736 V vs. $Fc^{+/0}$; i.e., zero overpotential). Bottom: 2D ground state free energy plot of ECEC mechanism based on arrows derived from the 3D plot.

Scheme 3. Proposed ECEC Mechanism for H_2 production using 1-Fe(NCMe)$^+$ and Tos_2NH in MeCN.[a]

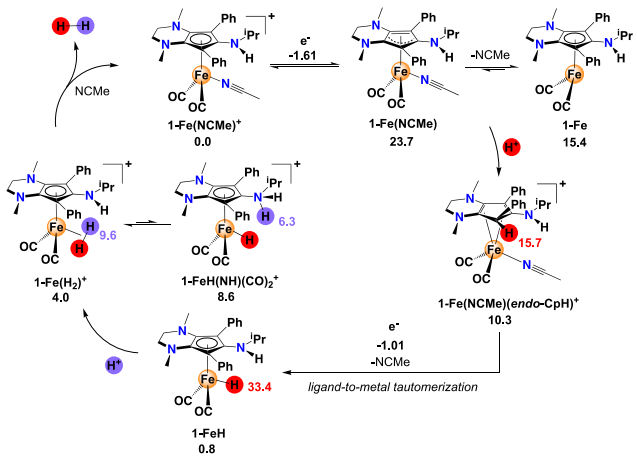

[a] Associated pK_a^{MeCN} values (red, purple) reduction potentials (black, V relative to $Fc^{+/0}$) are also shown. Ground state free energies are shown in black relative to **1-Fe(NCMe)**$^+$ (0.0 kcal/mol) at zero overpotential for the reaction $2Tos_2NH + 2e^- \rightleftharpoons H_2 + 2Tos_2N^-$ ($E°_{H+/H2}$ = -0.736 V vs. $Fc^{+/0}$). See Fig S28-S30 for tabulated free energies and pK_a^{MeCN} values of all other species considered.

CONCLUSION

In summary, we present a series of novel amine-rich monometallic iron electrocatalysts. Due to slow CO dissociation from the coordinatively saturated iron tricarbonyl precursors, one CO ligand is selectively extruded to afford electrocatalysts with H_2 production rates of up to 45 s^{-1} at room temperature. High-level computational investigation reveals that the commonly accepted paradigm of amine-assisted proton delivery and removal is likely not operative, underpinning the need to use comprehensive thermochemical landscape analyses for this mechanistically divergent electrocatalyst family.

ASSOCIATED CONTENT

Supporting Information

The Supporting Information is available free of charge on the ACS Publications website.

Experimental details, syntheses, NMR spectra, electrochemistry, DFT computational workflow (PDF)
Crystallographic data (CIF)
Computed Cartesian coordinates (XYZ)

AUTHOR INFORMATION

Corresponding Authors

* demyan.prokopchuk@rutgers.edu (D.E.P)
* hansen@thch.uni-bonn.de (A.H.)

Author Contributions

The authors declare no competing financial interest. All authors have given approval to the final version of the manuscript.
§These authors contributed equally.

ACKNOWLEDGMENT

D.E.P. thanks the National Science Foundation (NSF) for support under Grant 2055097 and S. G. thanks the Deutsche Forschungsgemeinschaft (DFG) under Grant 1927/16-1. This research was also supported by a Rutgers University-Newark startup grant (D.E.P.). X-ray structural solutions were partly supported by the NSF under Grant 2018753. D.E.P. thanks Prof. Robert Morris, Dr. R. Morris Bullock, and Prof. Mark Lipke for constructive suggestions.

REFERENCES

(1) (a) Lubitz, W.; Ogata, H.; Rüdiger, O.; Reijerse, E. Hydrogenases. *Chem. Rev.* **2014**, *114*, 4081-4148; (b) Evans, R. M.; Brooke, E. J.; Wehlin, S. A. M.; Nomerotskaia, E.; Sargent, F.; Carr, S. B.; Phillips, S. E. V.; Armstrong, F. A. Mechanism of hydrogen activation by [NiFe] hydrogenases. *Nat. Chem. Biol.* **2015**, *12*; (c) Wodrich, M. D.; Hu, X. Natural inspirations for metal-ligand cooperative catalysis. *Nat. Rev. Chem.* **2017**, *2*, 0099.

(2) (a) Helm, M. L.; Stewart, M. P.; Bullock, R. M.; DuBois, M. R.; DuBois, D. L. A Synthetic Nickel Electrocatalyst with a Turnover Frequency Above 100,000 s^{-1} for H_2 Production. *Science* **2011**, *333*, 863-866; (b) Yang, J. Y.; Bullock, R. M.; DuBois, M. R.; DuBois, D. L. Fast and efficient molecular electrocatalysts for H_2 production: Using hydrogenase enzymes as guides. *MRS Bull.* **2011**, *36*, 39-47; (c) O'Hagan, M.; Ho, M.-H.; Yang, J. Y.; Appel, A. M.; DuBois, M. R.; Raugei, S.; Shaw, W. J.; DuBois, D. L.; Bullock, R. M. Proton Delivery and Removal in $[Ni(PR_2NR'_2)_2]^{2+}$ Hydrogen Production and Oxidation Catalysts. *J. Am. Chem. Soc.* **2012**, *134*, 19409-19424; (d) Rauchfuss, T. B. Diiron Azadithiolates as Models for the [FeFe]-Hydrogenase Active Site and Paradigm for the Role of the Second Coordination Sphere. *Acc. Chem. Res.* **2015**, *48*, 2107-2116; (e) Schilter, D.; Camara, J. M.; Huynh, M. T.; Hammes-Schiffer, S.; Rauchfuss, T. B. Hydrogenase Enzymes and Their Synthetic Models: The Role of Metal Hydrides. *Chem. Rev.* **2016**, *116*, 8693-8749; (f) Bullock, R. M.; Chen, J. G.; Gagliardi, L.; Chirik, P. J.; Farha, O. K.; Hendon, C. H.; Jones, C. W.; Keith, J. A.; Klosin, J.; Minteer, S. D.; Morris, R. H.; Radosevich, A. T.; Rauchfuss, T. B.; Strotman, N. A.; Vojvodic, A.; Ward, T. R.; Yang, J. Y.; Surendranath, Y. Using nature's blueprint to expand catalysis with Earth-abundant metals. *Science* **2020**, *369*, eabc3183.

(3) (a) Yang, J. Y.; Smith, S. E.; Liu, T.; Dougherty, W. G.; Hoffert, W. A.; Kassel, W. S.; DuBois, M. R.; DuBois, D. L.; Bullock, R. M. Two Pathways for Electrocatalytic Oxidation of Hydrogen by a Nickel Bis(diphosphine) Complex with Pendant Amines in the Second Coordination Sphere. *J. Am. Chem. Soc.* **2013**, *135*, 9700-9712; (b) Dolui, D.; Khandelwal, S.; Shaik, A.; Gaat, D.; Thiruvenkatam, V.; Dutta, A. Enzyme-Inspired Synthetic Proton Relays Generate Fast and Acid-Stable Cobalt-Based H_2 Production Electrocatalysts. *ACS Catal.* **2019**, *9*, 10115-10125; (c) Slater, J. W.; Marguet, S. C.; Gray, M. E.; Monaco, H. A.; Sotomayor, M.; Shafaat, H. S. Power of the Secondary Sphere: Modulating Hydrogenase Activity in Nickel-Substituted Rubredoxin. *ACS Catal.* **2019**, *9*, 8928-8942; (d) Ghosh, P.; de Vos, S.; Lutz, M.; Gloaguen, F.; Schollhammer, P.; Moret, M.-E.; Klein Gebbink, R. J. M. Electrocatalytic Proton Reduction by a Cobalt Complex Containing a Proton-Responsive Bis(alkylimdazole)methane Ligand: Involvement of a C−H Bond in H_2 Formation. *Chemistry — A European Journal* **2020**, *26*, 12560-12569.

(4) (a) Chen, S.; Ho, M.-H.; Bullock, R. M.; DuBois, D. L.; Dupuis, M.; Rousseau, R.; Raugei, S. Computing Free Energy Landscapes: Application to Ni-based Electrocatalysts with Pendant Amines for H_2 Production and Oxidation. *ACS Catal.* **2014**, *4*, 229-242; (b) Raugei, S.; DuBois, D. L.; Rousseau, R.; Chen, S.; Ho, M.-H.; Bullock, R. M.; Dupuis, M. Toward Molecular Catalysts by Computer. *Acc. Chem. Res.* **2015**, *48*, 248-255.

(5) (a) Johnson, S. I.; Gray, H. B.; Blakemore, J. D.; Goddard, W. A. Role of Ligand Protonation in Dihydrogen Evolution from a Pentamethylcyclopentadienyl Rhodium Catalyst. *Inorg. Chem.* **2017**, *56*, 11375-11386; (b) Alférez, M. G.; Moreno, J. J.; Hidalgo, N.; Campos, J. Reversible Hydride Migration from C_5Me_5 to RhI Revealed by a Cooperative Bimetallic Approach. *Angew. Chem. Int. Ed.* **2020**; (c) Moreno, J. J.; Espada, M. F.; Campos, J.; López-Serrano, J.; Macgregor, S. A.; Carmona, E. Base-Promoted, Remote C–H Activation at a Cationic (η_5-C_5Me_5)Ir(III) Center Involving Reversible C–C Bond Formation of Bound C5Me5. *J. Am. Chem. Soc.* **2019**, *141*, 2205-2210.

(6) Kurtz, D. A.; Dhar, D.; Elgrishi, N.; Kandemir, B.; McWilliams, S. F.; Howland, W. C.; Chen, C.-H.; Dempsey, J. L. Redox-Induced Structural Reorganization Dictates Kinetics of Cobalt(III) Hydride Formation via Proton-Coupled Electron Transfer. *J. Am. Chem. Soc.* **2021**, *143*, 3393-3406.

(7) Jones, W. D.; Kuykendall, V. L.; Selmeczy, A. D. Ring migration reactions of $(C_5Me_5)Rh(PMe_3)H_2$. Evidence for η^3 slippage and metal-to-ring hydride migration. *Organometallics* **1991**, *10*, 1577-1586.

(8) Jones, W. D.; Rosini, G. P.; Maguire, J. A. Photochemical C−H Activation and Ligand Exchange Reactions of $CpRe(PPh_3)_2H_2$. Phosphine Dissociation Is Not Involved. *Organometallics* **1999**, *18*, 1754-1760.

(9) Kefalidis, C. E.; Perrin, L.; Burns, C. J.; Berg, D. J.; Maron, L.; Andersen, R. A. Can a pentamethylcyclopentadienyl ligand act as a proton-relay in f-element chemistry? Insights from a joint experimental/theoretical study. *Dalton Trans.* **2015**, *44*, 2575-2587.

(10) (a) Davison, A.; Green, M. L. H.; Wilkinson, G. 620. π-Cyclopentadienyl- and cyclopentadiene-iron carbonyl complexes. *J. Chem. Soc.* **1961**, 3172-3177; (b) Schild, D. J.; Drover, M. W.; Oyala, P. H.; Peters, J. C. Generating Potent C-H PCET Donors: Ligand-Induced Fe-to-Ring Proton Migration from a Cp^*Fe^{III}--H Complex Demonstrates a Promising Strategy. *J. Am. Chem. Soc.* **2020**, *142*, 18963-18970.

(11) (a) Green, M. L. H.; Pratt, L.; Wilkinson, G. 760. A new type of transition metal–cyclopentadiene compound. *J. Chem. Soc.* **1959**, 3753-3767; (b) Chalkley, M. J.; Oyala, P. H.; Peters, J. C. Cp* Noninnocence Leads to a Remarkably Weak C-H Bond via Metallocene Protonation. *J. Am. Chem. Soc.* **2019**, *141*, 4721-4729.

(12) (a) Gusev, O. V.; Denisovich, L. I.; Peterleitner, M. G.; Rubezhov, A. Z.; Ustynyuk, N. A.; Maitlis, P. M. Electrochemical generation of 19- and 20-electron rhodocenium complexes and their properties. *J. Organomet. Chem.* **1993**, *452*, 219-222; (b) Pitman, C. L.; Finster, O. N. L.; Miller, A. J. M. Cyclopentadiene-mediated hydride transfer from rhodium complexes. *Chem. Commun.* **2016**; (c) Quintana, L. M. A.; Johnson, S. I.; Corona, S. L.; Villatoro, W.; Goddard, W. A.; Takase, M. K.; VanderVelde, D. G.; Winkler, J. R.; Gray, H. B.; Blakemore, J. D. Proton-hydride tautomerism in hydrogen evolution catalysis. *Proc. Natl. Acad. Sci. U.S.A.* **2016**, *113*, 6409-6414; (d) Peng, Y.; Ramos-Garcés, M. V.; Lionetti, D.; Blakemore, J. D. Structural and Electrochemical Consequences of [Cp*] Ligand Protonation. *Inorg. Chem.* **2017**, *56*, 10824-10831.

(13) (a) Henke, W. C.; Lionetti, D.; Moore, W. N. G.; Hopkins, J. A.; Day, V. W.; Blakemore, J. D. Ligand Substituents Govern the Efficiency and Mechanistic Path of Hydrogen Production with [Cp*Rh] Catalysts. *ChemSusChem* **2017**, *10*, 4589-4598; (b) Chalkley, M. J.; Del Castillo, T. J.; Matson, B. D.; Peters, J. C. Fe-Mediated Nitrogen Fixation with a Metallocene Mediator: Exploring pK_a Effects and Demonstrating Electrocatalysis. *J. Am. Chem. Soc.* **2018**, *140*, 6122-6129; (c) Chalkley, M. J.; Del Castillo, T. J.; Matson, B. D.; Roddy, J. P.; Peters, J. C. Catalytic N_2-to-NH_3 Conversion by Fe at Lower Driving Force: A Proposed Role for Metallocene-Mediated PCET. *ACS Cent. Sci.* **2017**, *3*, 217-223.

(14) (a) Choi, J. H.; Kim, Y. H.; Nam, S. H.; Shin, S. T.; Kim, M.-J.; Park, J. Aminocyclopentadienyl Ruthenium Chloride: Catalytic Racemization and Dynamic Kinetic Resolution of Alcohols at Ambient Temperature. *Angew. Chem. Int. Ed.* **2002**, *41*, 2373-2376; (b) Casey, C. P.; Vos, T. E.; Singer, S. W.; Guzei, I. A. Protonated Aminocyclopentadienyl Ruthenium Hydride Reduction of Benzaldehyde and the Conversion of the Resulting Ruthenium Triflate to a Ruthenium Hydride with H_2 and Base.

Organometallics **2002**, *21*, 5038-5046; (c) Lator, A.; Gaillard, Q. G.; Mérel, D. S.; Lohier, J.-F.; Gaillard, S.; Poater, A.; Renaud, J.-L. Room-Temperature Chemoselective Reductive Alkylation of Amines Catalyzed by a Well-Defined Iron(II) Complex Using Hydrogen. *J. Org. Chem.* **2019**, *84*, 6813-6829.
(15) (a) Bursch, M.; Hansen, A.; Pracht, P.; Kohn, J. T.; Grimme, S. Theoretical study on conformational energies of transition metal complexes. *Phys. Chem. Chem. Phys.* **2021**, *23*, 287-299; (b) Grimme, S.; Bohle, F.; Hansen, A.; Pracht, P.; Spicher, S.; Stahn, M. Efficient Quantum Chemical Calculation of Structure Ensembles and Free Energies for Nonrigid Molecules. *J. Phys. Chem. A* **2021**, *125*, 4039-4054.
(16) Gompper, R.; Glöckner, H. Stable Cyclopentadienylium Salts. *Angew. Chem. Int. Ed.* **1984**, *23*, 53-54.
(17) Catheline, D.; Astruc, D. Synthesis and characterization of $C_5(CH_3)_5Fe(CO)_3^+$ PF_6^- and $C_5(CH_3)_5Fe(CO)_2^-$ K^+. *J. Organomet. Chem.* **1982**, *226*, C52-C54.
(18) (a) Elgrishi, N.; Kurtz, D. A.; Dempsey, J. L. Reaction Parameters Influencing Cobalt Hydride Formation Kinetics: Implications for Benchmarking H_2-Evolution Catalysts. *J. Am. Chem. Soc.* **2017**, *139*, 239-244; (b) Savéant, J. M.; Costentin, C. *Elements of Molecular and Biomolecular Electrochemistry*; John Wiley & Sons, Ltd, 2019.
(19) Pevear, K. A.; Holl, M. M. B.; Carpenter, G. B.; Rieger, A. L.; Rieger, P. H.; Sweigart, D. A. Ligand Substitution at 19-Electron Centers and the Indenyl Effect in Organometallic Radicals. Electrocatalytic CO Substitution in (cyclopentadienyl)$Fe(CO)_3^+$ and (indenyl)$Fe(CO)_3^+$. *Organometallics* **1995**, *14*, 512-523.
(20) Nguyen, K. T.; Lane, E. E.; McMillen, C. D.; Pienkos, J. A.; Wagenknecht, P. S. Is Indenyl a Stronger or Weaker Electron Donor Ligand than Cyclopentadienyl? Opposing Effects of Indenyl Electron Density and Ring Slipping on Electrochemical Potentials. *Organometallics* **2020**, *39*, 670-678.
(21) (a) Artero, V.; Fontecave, M. Hydrogen evolution catalyzed by $CpFe(CO)_2$-based complexes. *C.R. Chim.* **2008**, *11*, 926-931; (b) Felton, G. A. N.; Vannucci, A. K.; Okumura, N.; Lockett, L. T.; Evans, D. H.; Glass, R. S.; Lichtenberger, D. L. Hydrogen Generation from Weak Acids: Electrochemical and Computational Studies in the $[(\eta^5\text{-}C_5H_5)Fe(CO)_2]_2$ System. *Organometallics* **2008**, *27*, 4671-4679; (c) Hemming, E. B.; Chan, B.; Turner, P.; Corcilius, L.; Price, J. R.; Gardiner, M. G.; Masters, A. F.; Maschmeyer, T. $[Fe(C_5Ar_5)(CO)_2Br]$ complexes as hydrogenase mimics for the catalytic hydrogen evolution reaction. *Appl. Catal., B* **2018**, *223*, 234-241.
(22) Kütt, A.; Tshepelevitsh, S.; Saame, J.; Lõkov, M.; Kaljurand, I.; Selberg, S.; Leito, I. Strengths of Acids in Acetonitrile. *Eur. J. Org. Chem.* **2021**, *2021*, 1407-1419.
(23) Dutta, A.; Appel, A. M.; Shaw, W. J. Designing electrochemically reversible H_2 oxidation and production catalysts. *Nat. Rev. Chem.* **2018**, *2*, 244-252.
(24) Although the origins of these modest Faradaic efficiencies remain unclear, preliminary data suggests that slow reductive decomposition of exogenous acid is occurring. Work is ongoing to identify the post-electrolysis product(s).
(25) Appel, A. M.; Helm, M. L. Determining the Overpotential for a Molecular Electrocatalyst. *ACS Catal.* **2014**, *4*, 630-633.
(26) Kaljurand, I.; Kütt, A.; Sooväli, L.; Rodima, T.; Mäemets, V.; Leito, I.; Koppel, I. A. Extension of the Self-Consistent Spectrophotometric Basicity Scale in Acetonitrile to a Full Span of 28 pK_a Units: Unification of Different Basicity Scales. *J. Org. Chem.* **2005**, *70*, 1019-1028.
(27) Pracht, P.; Bohle, F.; Grimme, S. Automated exploration of the low-energy chemical space with fast quantum chemical methods. *Phys. Chem. Chem. Phys.* **2020**, *22*, 7169-7192.
(28) (a) Bannwarth, C.; Ehlert, S.; Grimme, S. GFN2-xTB - An Accurate and Broadly Parametrized Self-Consistent Tight-Binding Quantum Chemical Method with Multipole Electrostatics and Density-Dependent Dispersion Contributions. *J. Chem. Theory Comput.* **2019**, *15*, 1652-1671; (b) Bannwarth, C.; Caldeweyher, E.; Ehlert, S.; Hansen, A.; Pracht, P.; Seibert, J.; Spicher, S.; Grimme, S. Extended tight-binding quantum chemistry methods. *WIREs Comput. Mol. Sci.* **2021**, *11*, e1493.
(29) Grimme, S.; Hansen, A.; Ehlert, S.; Mewes, J.-M. r^2SCAN-3c: A "Swiss army knife" composite electronic-structure method. *J. Chem. Phys* **2021**, *154*, 064103.
(30) Sinnecker, S.; Rajendran, A.; Klamt, A.; Diedenhofen, M.; Neese, F. Calculation of Solvent Shifts on Electronic g-Tensors with the Conductor-Like Screening Model (COSMO) and Its Self-Consistent Generalization to Real Solvents (Direct COSMO-RS). *J. Phys. Chem. A* **2006**, *110*, 2235-2245.
(31) (a) Furness, J. W.; Kaplan, A. D.; Ning, J.; Perdew, J. P.; Sun, J. Accurate and Numerically Efficient r^2SCAN Meta-Generalized Gradient Approximation. *J. Phys. Chem. Lett.* **2020**, *11*, 8208-8215; (b) Ehlert, S.; Huniar, U.; Ning, J.; Furness, J. W.; Sun, J.; Kaplan, A. D.; Perdew, J. P.; Brandenburg, J. G. r^2SCAN-D4: Dispersion corrected meta-generalized gradient approximation for general chemical applications. *J. Chem. Phys* **2021**, *154*, 061101.
(32) Weigend, F.; Ahlrichs, R. Balanced basis sets of split valence, triple zeta valence and quadruple zeta valence quality for H to Rn: Design and assessment of accuracy. *Phys. Chem. Chem. Phys.* **2005**, *7*, 3297-3305.
(33) Spicher, S.; Grimme, S. Single-Point Hessian Calculations for Improved Vibrational Frequencies and Rigid-Rotor-Harmonic-Oscillator Thermodynamics. *J. Chem. Theory Comput.* **2021**, *17*, 1701-1714.
(34) (a) Klamt, A. Conductor-like Screening Model for Real Solvents: A New Approach to the Quantitative Calculation of Solvation Phenomena. *J. Phys. Chem.* **1995**, *99*, 2224-2235; (b) Klamt, A.; Jonas, V.; Bürger, T.; Lohrenz, J. C. W. Refinement and Parametrization of COSMO-RS. *J. Phys. Chem. A* **1998**, *102*, 5074-5085.
(35) Neugebauer, H.; Bohle, F.; Bursch, M.; Hansen, A.; Grimme, S. Benchmark Study of Electrochemical Redox Potentials Calculated with Semiempirical and DFT Methods. *J. Phys. Chem. A* **2020**, *124*, 7166-7176.
(36) It may also be possible that a concerted proton-electron transfer (CPET) directly converts **FeCpN+** to an *endo* protonated intermediate, circumventing these two compounds entirely.
(37) (a) Casey, C. P.; Guan, H. An Efficient and Chemoselective Iron Catalyst for the Hydrogenation of Ketones. *J. Am. Chem. Soc.* **2007**, *129*, 5816-5817; (b) Casey, C. P.; Guan, H. Cyclopentadienone Iron Alcohol Complexes: Synthesis, Reactivity, and Implications for the Mechanism of Iron-Catalyzed Hydrogenation of Aldehydes. *J. Am. Chem. Soc.* **2009**, *131*, 2499-2507; (c) Conley, B. L.; Pennington-Boggio, M. K.; Boz, E.; Williams, T. J. Discovery, Applications, and Catalytic Mechanisms of Shvo's Catalyst. *Chem. Rev.* **2010**, *110*, 2294-2312.